Atmospheric Environment 267 (2021) 118766

Contents lists available at ScienceDirect

Atmospheric Environment

journal homepage: www.elsevier.com/locate/atmosenv

Ensemble projection of global isoprene emissions by the end of 21st century using CMIP6 models

Yang Cao [a,b], Xu Yue [c,*], Hong Liao [c], Yang Yang [c], Jia Zhu [c], Lei Chen [c], Chenguang Tian [a,b], Yadong Lei [a,b], Hao Zhou [a,b], Yimian Ma [a,b]

[a] Climate Change Research Center, Institute of Atmospheric Physics (IAP), Chinese Academy of Sciences (CAS), Beijing, 100029, China
[b] University of Chinese Academy of Sciences, Beijing, China
[c] Jiangsu Key Laboratory of Atmospheric Environment Monitoring and Pollution Control, Collaborative Innovation Center of Atmospheric Environment and Equipment Technology, School of Environmental Science and Engineering, Nanjing University of Information Science & Technology (NUIST), Nanjing, 210044, China

HIGHLIGHTS

- CMIP6 models predict similar present-day isoprene emissions but varied trends.
- Isoprene emissions are projected to increase by 21–57% at the end of century.
- Temperature instead of CO_2 dominates the enhancement of isoprene emissions.

ARTICLE INFO

Keywords:
Isoprene
CMIP6
Multi-model ensemble
SSPs
Uncertainty

ABSTRACT

Isoprene is a key biogenic volatile organic compound of vital importance for global climate change and air quality. Previous studies projecting future changes of isoprene emissions showed a wide range of uncertainties due to the discrepancies in emission schemes, climate models, and future scenarios. Here, we use an ensemble of models from the Coupled Model Intercomparison Project version 6 (CMIP6) to explore the spatiotemporal variations of global isoprene emissions at present day and their changes by the end of 21st century. At present day, most models predict similar emission rates of 400 Tg C yr^{-1} but with large differences in the long-term trends. For models using the scheme of Model of Emissions of Gases and Aerosols from Nature, isoprene emissions show limited changes during historical period but significant enhancements after the year 2000. However, for models using another scheme with strong CO_2 inhibition effects, isoprene emissions show decreasing trends during historical period and moderate increasing trends after the year 2000. By the end of 21st century, the ensemble projection shows increases of 21–57% in isoprene emissions with the largest enhancement for the strongest warming scenario. Attribution shows that temperature is the dominant driver for the increase of isoprene emissions, no matter whether the CO_2 inhibition effects are considered or not. The enhanced isoprene emissions increase the risks of ozone pollution in a warmer climate.

1. Introduction

Biogenic volatile organic compounds (BVOCs) are important for global climate change and air quality (Fehsenfeld et al., 1992; Atkinson and Arey, 1998; Penuelas and Staudt, 2010; Jiang et al., 2018). Isoprene (2-methyl-1,3-butadiene, C5H8) is one of the dominant BVOCs emitted from vegetation (Pacifico et al., 2009). Global emissions of biogenic isoprene are estimated to be 400–600 Tg C yr^{-1} (see Table 1 in *Arneth et al. (2008)*), contributing to approximately half of the total BVOCs (about 1000 Tg C yr^{-1}, (Guenther et al., 2006)). Lifetime of isoprene is short from minutes to hours (Guenther et al., 1995) because of its strong reactivity in the troposphere. For example, isoprene promotes the formation of tropospheric ozone through photochemical reactions when NO_x levels are high (Goldstein et al., 2004; Velikova et al., 2005; Fu and Liao, 2012; Situ et al., 2013). Reduced isoprene will increase tropospheric OH concentrations, thereby decreasing the atmospheric lifetime of methane (Ortega et al., 2007; Arneth et al., 2008; Guenther et al., 2015). In addition, isoprene oxidation products can enhance the

* Corresponding author.
E-mail address: yuexu@nuist.edu.cn (X. Yue).

https://doi.org/10.1016/j.atmosenv.2021.118766
Received 29 June 2021; Received in revised form 8 September 2021; Accepted 26 September 2021
Available online 29 September 2021
1352-2310/© 2021 Elsevier Ltd. All rights reserved.

formation of secondary organic aerosols (SOA) by forming condensable products which are required for SOA growth (Claeys et al., 2004; Lim et al., 2005; Arneth et al., 2008).

Observations of isoprene emissions are sparce in both space and time because of its short lifetime. The limited measurements show the sensitive responses of isoprene emissions to environmental conditions. High temperature and radiation increase isoprene emissions (Tingey et al., 1979; Sharkey et al., 1996; Rinne et al., 2002; Stavrakou et al., 2014; Hantson et al., 2017). CO_2 promotes plant photosynthesis but suppress isoprene emissions (Arneth et al., 2007a; Wilkinson et al., 2009; Young et al., 2009; Lathiere et al., 2010; Possell and Hewitt, 2011). Furthermore, environmental conditions like plant water stress, ambient ozone and biotic stress also affect isoprene emissions (Sharkey and Loreto, 1993; Llusia et al., 2002; Penuelas and Staudt, 2010).

Based on these observed relationships, empirical schemes have been developed to estimate the regional and global isoprene emissions since the early 1990s (Guenther et al., 1995, 2012; Lamb et al., 1996; Niinemets et al., 1999; Arneth et al., 2007b; Grote and Niinemets, 2008; Pacifico et al., 2011; Unger et al., 2013; Grote et al., 2014), and have been routinely embedded in chemistry and climate models, for example WRF-Chem (Grell et al., 2005) and ECHAM6-HAMMOZ (Henrot et al., 2017). However, simulated isoprene emissions vary from study to study (Arneth et al., 2008; Guenther et al., 2012). Such uncertainties are partly caused by the differences in schemes and/or meteorological driving fields (Levis et al., 2003; Muller et al., 2008; Guenther et al., 2012; Yue et al., 2015), and may further cause discrepancies in assessing the environmental impacts of isoprene.

Given the essential roles of isoprene in atmospheric chemistry and climate change, many studies have projected the spatiotemporal variations of isoprene emissions in the future (Table 1). For example, Pacifico et al. (2012) simulated global annual isoprene emissions of 579, 460, and 456 Tg C yr^{-1} respectively at preindustrial, present-day, and by the year 2100 under RCP8.5 climate scenarios, with a process-based isoprene emission model implemented in the HadGEM2 Earth-system model. They reported that increased emissions resulting from climate warming could be offset by the CO_2 inhibition effect. Hantson et al. (2017) performed simulations using the dynamic global vegetation model LPJ-GUESS over the period 1901–2100 and found that future global isoprene emissions are strongly dependent on the climate and land use scenarios. Furthermore, the present-day average emission of 385 Tg C yr^{-1} will increase by 159 Tg C yr^{-1} by the year 2100 under the RCP4.5 scenario, but instead decrease by 8 Tg C yr^{-1} if CO_2 inhibition effect is considered.

Previous projections show a wide range of uncertainties in future changes of isoprene emissions ranging from −259 to 1344 Tg C yr^{-1} (Table 1), because of the discrepancies in emission schemes, climate models, future scenarios, CO_2 effects, and land cover changes considered. Multi-model ensemble is an effective approach to explore the uncertainties in climate projections, and has been widely used by the Intergovernmental Panel on Climate Change (IPCC) assessment reports based on output from the Coupled Model Intercomparison Project (CMIP) (IPCC et al., 2007, 2014). The latest phase of CMIP, the version

Table 1
Summary of studies projecting future changes in isoprene emissions.

References	Time	Isoprene Scheme[a]	Climate Model	CO_2 effect	LCC	Scenarios[b]	Changes (Tg C yr^{-1})
Sanderson et al. (2003)	2090s	G1995	HadCM3	NO	NO	SRES A2	165
				NO	YES		130.6
Lathiere et al. (2005)	2100	G1995	LMDz	NO	YES	/	136
Liao et al. (2006)	2100	G1995	GISS GCM II′	NO	NO	SRES A2	242.5
Wiedinmyer et al. (2006)	2070–2099	G1995	HADCM2SUL	NO	YES	/	323.8
Heald et al. (2008)	2100	G2006	CCSM3	NO	NO	SRES A1B	111
Heald et al. (2009)	2100	G2006;	CCSM3	YES	YES	SRES A1B	719
		W2009		YES	NO		−44
				NO	YES		1344
				NO	NO		188
Young et al. (2009)	2090s	N1999	HadCM3	YES	NO	SRES A2	−55
				NO	NO		363
Ganzeveld et al. (2010)	2050	G1995	ECHAM5	NO	YES	SRES A2	−49
Pacifico et al. (2012)	2100–2109	P2011	HadGEM2	YES	YES	RCP8.5	−4
				NO	YES		399
				YES	YES	RCP2.6	1
Wu et al. (2012)	2050	G2006	GISS GCM3	NO	YES	SRES A1B	−19
	2100						36
	2050			NO	NO		31
	2100						103
Tai et al. (2013)	2050	G2012	GISS GCM3	YES	YES	SRES A1B	−15
				YES	NO		19
				NO	YES		137
				NO	NO		183
Squire et al. (2014)	2095	G2006 ;	HadGEM3	YES	YES	SRES B2	−259
		P2005		NO	NO		78
Lin et al. (2016)	2100	G2012	CESM v 1.2.2	YES	NO	RCP8.5	94
				YES	YES		42
Hantson et al. (2017)	2071–2100	N1999	MPI	YES	YES	RCP4.5	−8
				NO	YES		159
Szogs et al. (2017)	2091–2100	N1999	IPSL-CM5A-LR	YES	YES	RCP2.6	−19.2
Rabin et al. (2020)	2091–2100	G2012	IPSL-CM5A-MR	YES	YES	SSP145	−44
						SSP360	−125
						SSP460	−99
						SSP585	−118
Wang et al. (2020)	2050	G2012	CESM v1.2	NO	YES	RCP4.5	22.6
						RCP8.5	−32.5

[a] Isoprene schemes includes G1995 Guenther et al. (1995), G2006 Guenther et al. (2006), W2009 Wilkinson et al. (2009), N1999 Niinemets et al. (1999), P2011 Pacifico et al. (2011), G2012 Guenther et al. (2012), and P2005 Possell et al. (2005).

[b] Scenarios include SRES from IPCC Assessment Report 4 (AR4), RCP from IPCC AR5, and SSP from IPCC AR6. The higher the numbers, the warmer the scenarios. For example, RCP8.5 is warmer than RCP4.5.

6, for the first time provides simulations of isoprene emissions from multiple chemistry-climate coupled models, facilitating the intercomparison of future projections within the same experimental settings.

In this paper, we explore the spatiotemporal variations of global isoprene emissions at present day and project their changes by the end of 21st century using the ensemble simulations from CMIP6 models. The major objectives are to: (1) identify the dominant drivers of the changes in future isoprene emissions and (2) quantify the uncertainties of emission changes associated with different climate scenarios and emission schemes. We first evaluate the performance of climate models in simulating present-day climatology of isoprene emissions. We then compare the future changes of isoprene emissions at 4 Shared Socioeconomic Pathways (SSPs) to assess the uncertainties caused by climate scenarios. Finally, we identify the dominant drivers for isoprene changes from CO_2 effects and varied meteorological factors to explore the uncertainties induced by isoprene emission schemes.

2. Methods and data

2.1. Measurement data

Measurements of isoprene emissions from literature (Table S1) were collected through the Web of Science (https://apps.webofknowledge.com) using keywords like isoprene/BVOCs and measurement/observation/flux to evaluate the performance of CMIP6 models. More than three hundred literatures were found, among which 55 papers provided site locations, observational periods, and emission fluxes. The units of both measurements and simulations are converted to mg C m^{-2} day $^{-1}$ to facilitate the comparisons. We choose the latest observations if one site has multiple measurement samples and finally all the measurements collected were compiled at 49 sites, including 17 evergreen broadleaf forest (EBF), 6 evergreen needleleaf forest (ENF), 20 deciduous broadleaf forest (DBF), 1 shrubland (shrub), 4 grassland (grass), and 1 cropland (crop). Simulated isoprene emissions are interpolated to the specific locations where the measurement samples are collected and averaged over the same observing periods for comparisons.

2.2. Climate models from CMIP6 archive

We collected data from all the available CMIP6 models providing isoprene emissions for both present day and at least one future climate scenario. In total, 7 climate models with different isoprene emission schemes are selected (Table 2). CESM2-WACCM is a fully coupled Earth System Model using the Community Earth System Model version 2 (Emmons et al., 2020). Biogenic emissions are calculated by the Model of Emissions of Gases and Aerosols from Nature (MEGAN) version 2.1 (Guenther et al., 2012). GFDL-ESM4 is a coupled chemistry-carbon-climate Earth System Model developed by geophysical fluid dynamics laboratory (Dunne et al., 2020). Emissions of BVOCs are calculated online in AM4.1, an atmospheric model, using an earlier version of MEGAN (Guenther et al., 2006). GISS-E2-1-G is a climate model composed of the ModelE atmospheric model and the NASA Goddard Institute for Space Studies (GISS) ocean model (NASA/GISS., 2018). Isoprene emissions are calculated online and respond to temperature and radiation (Wang et al., 1998; Shindell et al., 2006). The Meteorological Research Institute Earth System Model version 2.0 (MRI-ESM2-0) is developed by the Japan Meteorological Agency (Yukimoto et al., 2019). It contains a chemistry module called MRI-CCM2, which calculates biogenic emissions using the scheme from Guenther et al. (1995).The Norwegian Earth System Model version 2 (NorESM2) is developed by the Norwegian Climate Center. NorESM2 has two versions: NorESM2-LM and NorESM2-MM, which are different in horizontal resolution and land components. LM has lower resolution of 1.9° × 2.5° than that of 0.9° × 1.25° in MM (Horowitz et al., 2003). Both versions of models calculate BVOCs emissions with MEGAN2.1. UKESM1-0-LL is UK's Earth System Model (Sellar et al., 2019). Emissions of $BVOC_S$ are calculates using the interactive biogenic VOC (iBVOC) emission model (Pacifico et al., 2011).

Table 2
Summary of CMIP6 models used in this study.

Models	Country	Resolution[a]	Scheme	Scenarios
CESM2-WACCM	USA	0.9° × 1.25°	G2012[b]	Historical,SSP370
GFDL-ESM4	USA	1° × 1.25°	G2006[c]	Historical,SSP126,SSP245, SSP370,SSP585
GISS-E2-1-G	USA	2° × 2.5°	G1995[d]	Historical,SSP126,SSP245, SSP370,SSP585
MRI-ESM2-0	Japan	2.8° × 2.8°	G1995	Historical,SSP126,SSP245, SSP370,SSP585
NorESM2-LM	Norway	1.9° × 2.5°	G2012	Historical,SSP126,SSP245, SSP370,SSP585
NorESM2-MM	Norway	0.9° × 1.25°	G2012	Historical,SSP126,SSP245, SSP370,SSP585
UKESM1-0-LL	UK	1.25° × 1.88°	P2011[e]	Historical,SSP370

[a] Latitude by Longitude.

2.3. Future climate scenarios

Scenario Model Intercomparison Project (ScenarioMIP) is one of the primary activities within CMIP6 deriving future climate and chemistry projections based on the Shared Socioeconomic Pathways (SSPs). The ScenarioMIP contains 4 main sets of future experiments including SSP126, SSP245, SSP370 and SSP585, which are differentiated by the magnitude of radiative forcing: SSP126 is the lowest warming scenario with radiative forcing of 2.6 W m^{-2} by the year 2100. SSP245 is a medium warming scenario with radiative forcing of 4.5 W m^{-2} by the year 2100. SSP370 is also a medium warming scenario but with higher radiative forcing of 7.0 W m^{-2} at the end of century. SSP585 is the highest warming scenario with radiative forcing of 8.5 W m^{-2} at 2100. These future scenarios are in general consistent with the Representative Concentration Pathways (RCP) applied by the CMIP5 but with some changes in the emission pathways of greenhouse gases.

All 7 models provide simulated isoprene emissions at present day and the future scenario of SSP370 (Table 2). Among them, 5 models perform future projections under additional scenarios including SSP126, SSP245, and SSP585. To identify the drivers of isoprene changes, we use auxiliary data including surface air temperature and surface downward radiation. Only three climate models (CESM2-WACCM, GFDL-ESM4 and MRI-ESM2-0) provide reasonable CO_2 concentrations that are consistent with the benchmark from IIASA (https://tntcat.iiasa.ac.at/SspDb). All simulation data are archived separately for historical period (1850–2014) and future scenarios (2015–2100) on the server of the Earth System Grid Federation (ESGF, https://esgf-index1.ceda.ac.uk/search/cmip6-ceda/). We interpolate spatial resolutions of different models into the same 1° × 1° to facilitate the aggregations and comparisons.

2.4. Isoprene emission schemes

Almost all emission schemes of isoprene can be summarized as follows:

$$E_i = f_T \cdot f_R \cdot \kappa_{CO_2} \cdot f_{others} \quad (1)$$

Here, E_i is the isoprene emission rate affected by many environmental factors including temperature (f_T), solar radiation (f_R), CO_2 (κ_{CO_2}) and others (f_{others}). Although the format of these components varies among different schemes (Table 3), the positive effects of temperature and radiation on emissions remain the same. Four models (CESM2-WACCM, NorESM2-LM, NorESM2-MM and UKESM1-0-LL) consider the impacts of CO_2 on isoprene emissions, while the rest three models (GFDL-ESM4, GISS-E2-1-G and MRI-ESM2-0) do not. For CO_2 effects,

Table 3
The format of different components in isoprene emission schemes[a].

Scheme	f_T	f_R	κ_{CO_2}	f_{others}
G1995	$\frac{exp\frac{c_{T1}(T_l-T_S)}{RT_ST_l}}{1+exp\frac{c_{T2}(T_l-T_M)}{RT_ST_l}}$	$\frac{\alpha_1 c_L Q}{\sqrt{1+\alpha_1{}^2Q^2}}$	/	/
G2006	$E_{opt}\cdot\frac{C_{T2}\cdot exp(C_{T1}x)}{C_{T2}-C_{T1}(1-exp(C_{T2}x))}$	$C_p\cdot\frac{\alpha\cdot PPFD}{\sqrt{1+\alpha^2PPFD^2}}$	/	$f_A\cdot f_{SM}$
P2011	$min(e^{a_T(T_a-T_{st})};2.3)$	$\frac{A_J+R_D}{(A_J)_{st}+R_{D_{st}}}$	$\frac{C_{i_{st}}}{C_i}$	/
G2012	$(1-LDF)\gamma_{T\_LIF}+LDF\cdot\gamma_{T\_LDF}$	$(1-LDF)+LDF\cdot\gamma_{P\_LDF}$	$I_{Smax}-\frac{I_{Smax}\cdot(C_i)^h}{(C^*)^h+(C_i)^h}$	$f_A\cdot f_{SM}$

[a] The descriptions of symbols and parameters are shown in Appendix A.

CESM2-WACCM, NorESM2-LM, and NorESM2-MM apply the inhibition parameterization proposed by Heald et al. (2009), while UKESM1-0-LL applies the parameterization of Niinemets et al. (1999).

2.5. Analyses

To estimate the changes in future isoprene emissions, we calculate the differences of projected emissions between the end of century (2080–2100) under four SSP scenarios and present day (1990–2010) using data from 5 climate models (GFDL-ESM4, GISS-E2-1-G, MRI-ESM2-0, NorESM2-LM, NorESM2-MM). To identify the main drivers of the projected changes in isoprene emissions, we select the data from all 7 models for both historical and SSP370 scenario. We apply the multiple linear regressions between isoprene emissions (E_i) and temperature (T), solar radiation (R), and CO_2 concentrations ([CO_2]) during 1980–2100 for the four models including CO_2 effects:

$$E_i = \kappa_{CO2}\cdot(a\cdot T + b\cdot R + c) \quad (2)$$

Here, k_{CO2} is the CO_2 scheme applied for different models (Table 3). We isolate CO_2 effect using k_{CO2} instead of a predictor in linear regression, because CO_2 can increase temperature and as a result has large collinearity with predictor T. For other three models without CO_2 effects, we derive the regressions based on T and R as follows:

$$E_i = a\cdot T + b\cdot R + c \quad (3)$$

We derive regression functions grid by grid and as a result the coefficients a, b, c are spatial matrixes. Similar methods have been used to identify the contributions of meteorological variables to perturbations in air pollution (Tai et al., 2012; Li et al., 2020), carbon fluxes (Piao et al., 2013), and ecosystem productivity (Cheng et al., 2015; Hemes et al., 2020). We then perform sensitivity experiments by allowing each time a single factor (T, R, or [CO2]) to interannually vary and other factors are fixed at the year 1980. By comparing the projected future changes in predictand by 2080–2100, we derive the contributions of individual factors to the changes of global isoprene emissions. We apply the same procedure for each climate model independently so that the regression coefficient matrixes are different. We compare and synthesize the derived ΔE_i from different climate models.

3. Results

3.1. Present-day isoprene emissions

We first evaluate the performance of CMIP6 models in simulating present-day isoprene emissions. The spatial correlation coefficients (R) between models and observations range from 0.18 to 0.45 for different models (Fig. 1a). Such low R indicates that current state-of-the-art models have difficulties in depicting the global distribution of isoprene emissions. Three models, CESM2-WACCM, NorESM2-LM, and NorESM2-MM, which calculate isoprene with MRGAN2.1, show similar R of 0.22–0.23 and high normalized standard deviations (standard deviation of the model divided by that of the observations) of 1.20–1.24 against observations. In contrast, the other models show relatively low normalized standard deviations (0.51–0.71), indicating smaller spatial variability than observations. The multi-model ensemble yields a low R of 0.32 with observations (Fig. 1b), suggesting that the ensemble

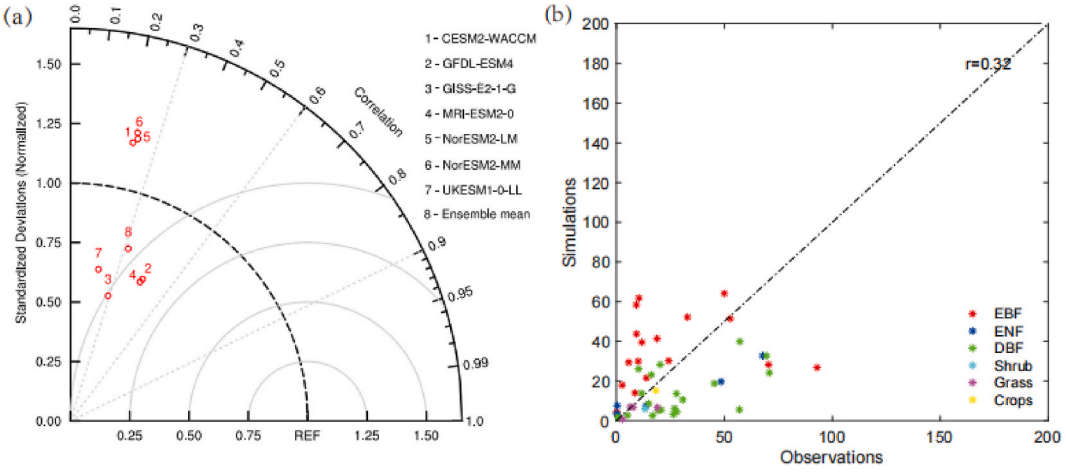

Fig. 1. Evaluations of isoprene simulations from CMIP6 models. Literature-based measurements are compared with (a) seven individual models and (b) multi-model ensemble during 1985–2014. Observational records (units: mg C m^{-2} day^{-1}) are shown for different plant functional types, including evergreen broadleaf forest (EBF), evergreen needleleaf forest (ENF), deciduous broadleaf forest (DBF), shrubland, grassland, and cropland. The correlation coefficient (r) is shown in the top right corner.

approach cannot improve the internal biases of single models. In general, simulated emissions are overestimated for EBF (by 45%) but underestimated for grassland (by 41.19%), ENF (by 43.99%), and DBF (by 51.89%). For example, the multi-model ensemble yields a prediction of 5.59 mg C m^{-2} day^{-1} for DBF emissions at Montmeyan in France ([43.6°N, 6.1°E]); such magnitude is only 10% of the observed 57 mg C m^{-2} day^{-1}. Such poor result is mainly caused by biases in mechanisms, uncertainties in meteorological forcings, and limitations in observations for model calibrations.

In addition to the biases in spatial distribution of isoprene emissions, simulated temporal variations also vary among models (Fig. S1a). Previous studies suggest a range of 400–600 Tg C yr^{-1} for present-day isoprene emissions (see Table 1 in Arneth et al. (2008)). Although the long-term mean values fall within such range (411–473 Tg C yr^{-1}) for all models, their trends vary a lot from 0.0 for MRI-ESM2-0 to 1.8 Tg C yr^{-2} for NorESM2-MM during 1980–2014. Such discrepancies are likely caused by the varied responses to temperature, radiation, and CO_2 for different emission schemes (Table 2). The simulated trends are similar for the models using the same schemes. For example, predicted trends are around 1.5 Tg C yr^{-2} for CESM2-WACCM, NorESM2-LM, NorESM2-MM which all use the G2012 scheme (Table 2).

3.2. Long-term variations of isoprene emissions

Global isoprene emissions show significant changes during 1850–2100 (Fig. 2a). For the historical period, the ensemble mean emission experiences small fluctuations from 402 to 463 Tg C yr^{-1} with small inter-model variability of 8–41 Tg C yr^{-1} during 1850–1980. After the year 1980, global emissions show an increasing trend of 0.49 Tg C yr^{-1} to the year 2014. The future projection continues to increase under four SSPs but with different rates. The largest growth rate is predicted under the SSP585 scenario, followed by the SSP370 and SSP245 scenarios. The modest rate is predicted for SSP126, which shows decreasing trend during 2050–2100. The increasing trends are similar (1.98–2.72 Tg C yr^{-1}) for the four SSPs during 2015–2050.

The changes of isoprene emissions mainly follow that of meteorological variables. Temperature shows a moderate trend of 0.001 °C yr^{-1} ($p < 0.01$) during 1850–1980 and a larger trend of 0.024 °C yr^{-1} ($p < 0.01$) during 1980–2014 (Fig. 2b). After the year 2014, the warming intensifies for all SSP scenarios with the largest rate for SSP585 (0.048 °C yr^{-1}) and the lowest for SSP126 (0.006 °C yr^{-1}), the latter of which peaks around the year 2050. Such temperature trends are correspondent to the changes of CO_2 concentrations (Fig. 2d). The ensemble shortwave radiation shows a decreasing trend of 0.024 W m^{-2} yr^{-1} ($p < 0.01$) from 1850 to 2014, because the enhanced anthropogenic aerosol loading dampens surface insolation (Wild, 2009; Kambezidis et al., 2012). Such dimming effect continues to intensify all through the 21st century in both SSP370 and SSP585 scenarios, but is largely alleviated in SSP126 (Fig. 2c).

We further examine the inter-model variability of the simulated isoprene emissions (Fig. 3). The model MRI-ESM2-0 shows no trends during 1850–2100, though this model exhibits the highest spatial R against observations at present day (Fig. 1a). As a result, we exclude this model in the following analyses. The model UKESM1-0-LL predicts a decreasing trend of 0.92 Tg C yr^{-2} ($p < 0.01$) during 1850–1980 (Fig. 3a), because of the combined effects of moderate dimming (Fig. 3c) and strong CO_2 inhibition (Fig. 3d). The same model projects an increasing trend of 0.62 Tg C yr^{-2} ($p < 0.01$) from 1980 to 2100, because the strong warming (Fig. 3b) overweighs the CO_2 inhibition effect. For the rest models, similar temporal variations are predicted with almost constant emissions during 1850–1980 and a significant enhancement thereafter (Fig. 3a). It worth noting that present-day estimates from all 7 models are quite similar (Fig. S1a), leading to large discrepancies in preindustrial and future periods among them.

3.3. Future changes in isoprene emissions

The multi-model ensemble predicts a global average emission of 448.2 Tg C yr^{-1} during 1990–2010 (Fig. 4a). Over 66.38% of isoprene emissions are located at the tropical regions (15°S-15°N), with hot spots over tropical rainforest. Such spatial pattern remains identical for more than one century, as the differences between preindustrial and present day are lower than 9.03% regionally and 4.25% globally (Fig. 4b). By end of this century, isoprene emissions increase largely especially in the tropical regions for the large emission base (Fig. 4c–f). Isoprene emissions in the tropical region increase by 20.51–61.61%, and the rest regions increase by 22.57–48.39%. The largest global enhancement is predicted under the SSP585 (256.2 Tg C yr^{-1}) scenario, followed by the

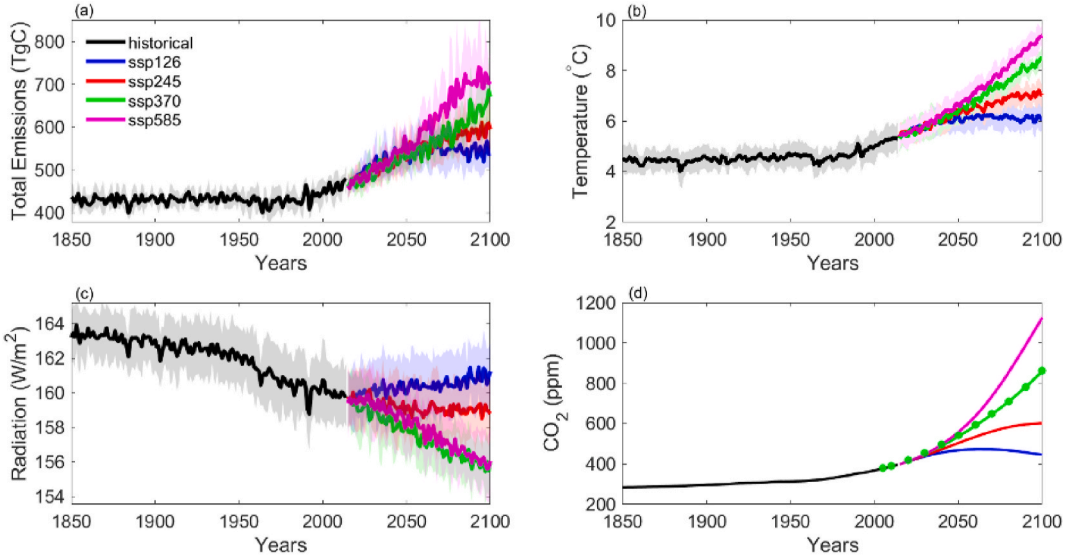

Fig. 2. Multi-model ensemble mean (a) global total isoprene emissions, (b) temperature, (c) shortwave radiation, and (d) CO_2 concentrations over the period 1850–2100. The shading shows one standard deviation of the inter-model variability. Results of (a–c) are derived using data from four models (GFDL-ESM4, GISS-E2-1-G, NorESM2-LM and NorESM2-MM). Results of (d) CO_2 concentrations are from three models (CESM2-WACCM, GFDL-ESM4 and MRI-ESM2-0). Green asterisks in (d) are offline CO_2 concentrations for ScenarioMIP SSP370 experiment (https://tntcat.iiasa.ac.at/SspDb). (For interpretation of the references to colour in this figure legend, the reader is referred to the Web version of this article.)

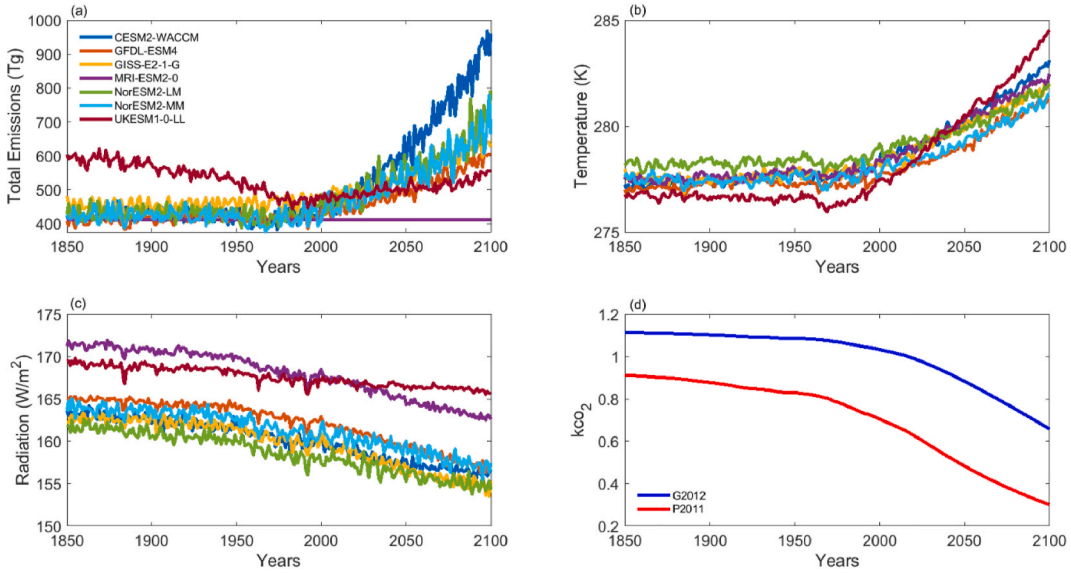

Fig. 3. Simulated temporal variations of global (a) total isoprene emissions, (b) mean temperature, (c) mean radiation, and (d) CO_2 inhibition factor (κ_{CO_2}) over the period 1850–2100 under SSP370 scenario. CO_2 inhibition factors are calculated with two different κ_{CO_2} (P2011 and G2012 in Table 1) using CO_2 concentrations from the same scenario.

SSP370 (183.4 Tg C yr^{-1}), SSP245 (140.6 Tg C yr^{-1}) and SSP126 (95.0 Tg C yr^{-1}) scenarios.

Projection of future isoprene change varies among models (Fig. 5). Under SSP370 scenario, CESM2-WACCMA predicts the largest increment of 427.68 Tg C yr^{-1}, which is more than twice as much as the ensemble mean of 203.78 Tg C yr^{-1}. In contrast, UKESM1-0-LL predicts the least increasement (61.27 Tg C yr^{-1}), only one third of the ensemble average. The difference is only 3.78% for the future isoprene changes between NorESM2-LM and NorESM2-MM, which employ the same physical scheme but with different resolutions.

3.4. Attribution of isoprene changes

Changes of isoprene emissions are jointly determined by the perturbations in temperature, radiation, and CO_2 concentrations. Regression analyses reproduce the projected changes in isoprene emissions, and decompose the contributions from individual factors under the SSP370 scenario (Fig. 5).

Radiation makes limited contributions to the changes of isoprene emissions, though global average radiation exhibits significant reductions during 1850–2100 (Fig. 3c). The spatial analyses also reveal that radiation-induced isoprene changes are trivial (Fig. S2) because radiation change is limited to the populated regions at middle latitudes (Fig. S4) while most of isoprene emissions are confined in the tropics (Fig. 4a).

Changes of CO_2 reduce isoprene emissions in four models that consider CO_2 effects. The three models, CESM2-WACCMA, NorESM2-LM, and NorESM2-MM, apply the same emission scheme of G2012, and as a result show similar negative contributions by CO_2. Predicted k_{CO2} reduces faster for P2011 than G2012 (Fig. 3d), leading to almost doubled CO_2 inhibition in UKESM1-0-LL relative to the above three models.

Temperature makes positive and dominant contributions in all 6 models. The largest contribution (808.50 Tg C yr^{-1}) by temperature is predicted for CESM2-WACCMA, which applies the same emission scheme of G2012 as NorESM2-LM, and NorESM2-MM. For 2015–2100, the CESM2-WACCMA projects a warming rate of 0.051 °C yr^{-1}, higher than that of 0.033 °C yr^{-1} by NorESM2-LM and 0.037 °C yr^{-1} by NorESM2-MM (Fig. 3b). The warming alone also largely increases isoprene emissions by 761.65 Tg C yr^{-1} in UKESM1-0-LL. However, such increment is weakened 36.23% by the negative effects of CO_2, leading to the lowest enhancement of isoprene emissions among the 6 models. For GFDL-ESM4 and GISS-E2-1-G which do not include CO_2 effects, the total emission increment is almost 100% attributed to the warming effect except for some minor offsets by radiation changes.

4. Conclusions and discussion

We applied multi-model output from the CMIP6 archive to project future changes in global isoprene emissions by the end of 21st century. Simulated long-term mean emissions are about 400 Tg C yr^{-1} at present day for most models, while the trends vary a lot among models (Fig. S1). For models using the MEGAN scheme, isoprene emissions show limited changes during historical period but significant enhancements after the year 2000 (Fig. 3). However, for models using the P2011 scheme, isoprene emissions show decreasing trends during historical period with moderate increasing trends after the year 2000. A dominant fraction of isoprene changes is located at the tropical region, where there is large forest coverage (Fig. 4). The projection shows some differences among future scenarios, with the largest growth rate under the SSP585 scenario and the lowest under the SSP126 scenario, the latter of which exhibits a downward trend during 2050–2100. Attribution analyses show that temperature is the dominant factor contributing to the changes of isoprene emissions, no matter whether the CO_2 inhibition effects are considered or not (Fig. 5).

Previous studies show a wide range of changes from −259 to 1344 Tg C yr^{-1} in the projection of future isoprene emissions (Table 1). Such uncertainty can be related to the differences in external forcings such as time periods, future scenarios, and climate models. First, the emissions in later periods are likely higher. Relative to the year 2050, isoprene emissions are projected to be higher by 55–72 Tg C yr^{-1} by the year 2100 (Wu et al., 2012). With CMIP6 data, we projected that isoprene emissions are higher by 72–165 Tg C yr^{-1} at the end of century than 2050 for different scenarios (SSP245, SSP370, SSP585). Such enhancement is likely associated with the warmer climate by 2100. Second, the projection is dependent on the climate scenarios. For studies using the G2012 scheme, isoprene emissions in the high-warming scenario (e.g., RCP8.5 or SSP585) are lower by 55–74 Tg C yr^{-1} than that in the moderate-warming scenario (e.g., RCP4.5 or SSP145) (Rabin et al., 2020; Wang et al., 2020). However, for CMIP6 projections using the

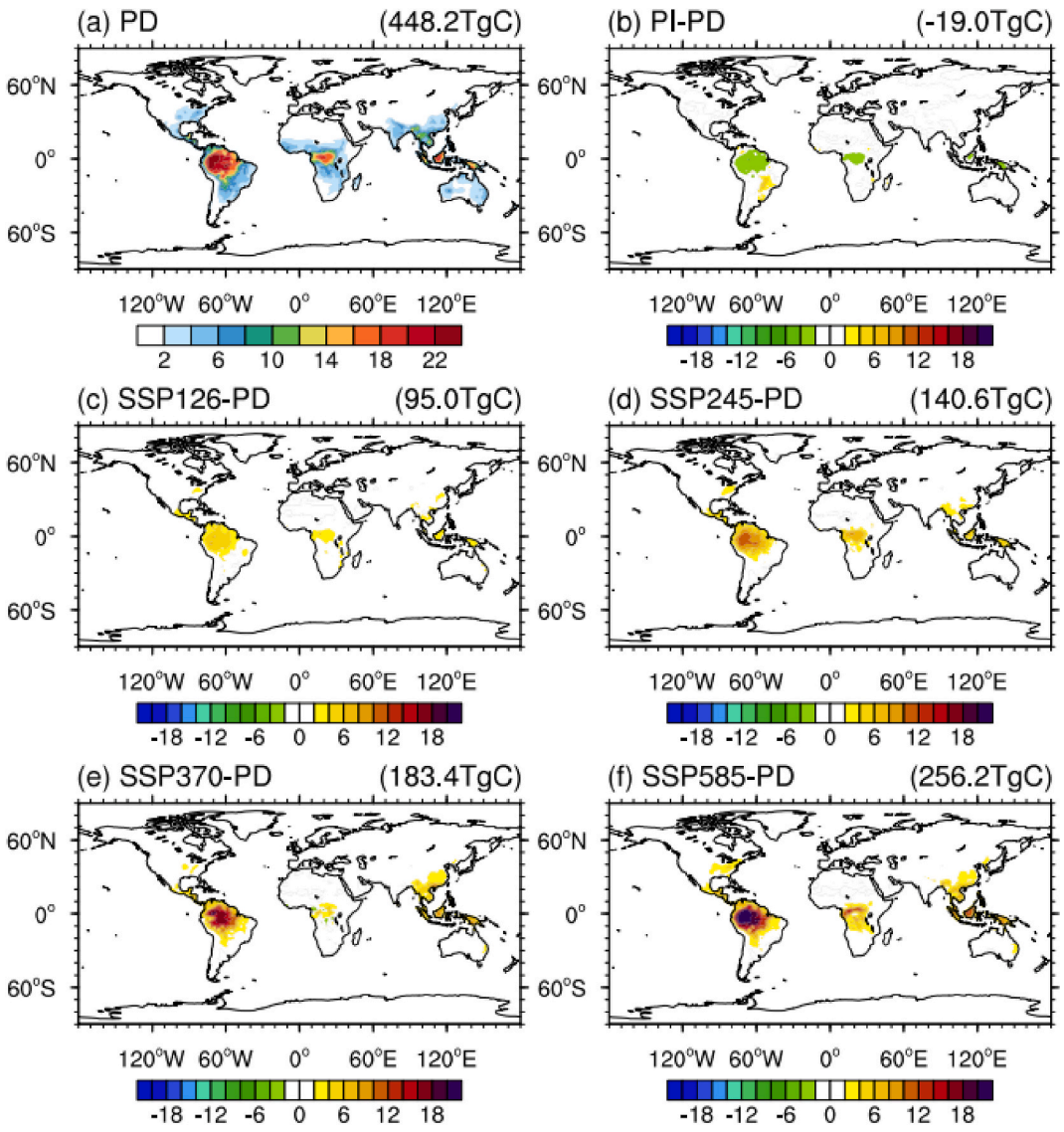

Fig. 4. Multi-model ensemble mean isoprene fluxes (g C m^{-2} a^{-1}) at (a) present day (PD, 1990–2010) and their changes at (b) pre-industry (PI, 1850–1870) and (c–f) four shared socioeconomic pathways (SSP126, SSP245, SSP370, SSP585, 2080–2100). Results are derived using data from four available models (GFDL-ESM4, GISS-E2-1-G, NorESM2-LM and NorESM2-MM). Global total isoprene emissions at present day and their changes at different periods are shown in the upper right corner of each plot.

same isoprene schemes, the emissions are higher by 82–148 Tg C yr^{-1} in SSP585 than that in SSP245 (Fig. 2a). The cause for such discrepancy remains unclear but is likely related to the different settings of CO_2 effects and land cover changes among studies. Third, future projections of isoprene are dependent on climate models. For example, with the same G1995 emission scheme and SRES A2 climate scenario, projected isoprene increment is higher by 88 Tg C yr^{-1} using GISS GCM (Liao et al., 2006) than that using HadCM3 (Sanderson et al., 2003). For CMIP6 models, the projected isoprene enhancement under the SSP370 scenario is almost doubled in CESM2-WACCM compared to NorESM2-LM, both of which employ the same G2012 scheme (Fig. 5).

Compared to the external forcings, differences of internal configurations such as physical parameterizations, CO_2 effects, and land cover change (LCC) may cause larger uncertainties for the future projections of isoprene emissions. For example, within the same modeling framework (climate model of GISS GCM3, time period of 2050, future scenario of SRES A1B), projections are higher by 150 Tg C yr^{-1} using G2012 (Tai et al., 2013) than that using G2006 (Wu et al., 2012) if the same CO_2 effects and LUC are applied. Such discrepancy is mainly caused by the varied temperature- and radiation-dependence of isoprene emissions. As a comparison, inclusion of CO_2 inhibition effects can lead to a reduction of 152–625 Tg C yr^{-1} relative to those without CO_2 effects (Heald et al., 2009; Young et al., 2009; Tai et al., 2013; Hantson et al., 2017). For CMIP6, models considering CO_2 effects project lower emissions of 137–276 Tg C yr^{-1} than those without CO_2 inhibition. Similarly, inclusion of future LCC projects lower isoprene emissions by 34–67 Tg C yr^{-1} than those using prescribed land cover (Sanderson et al., 2003; Wu et al., 2012; Tai et al., 2013; Lin et al., 2016). However, Heald et al. (2009) predicted higher emissions by 763–1156 Tg C yr^{-1} with LCC, because the global vegetation model they used projected doubled or even tripled forest coverage and leaf area index (LAI) due to CO_2 fertilization effects. Such enhancements in LAI are likely overestimated as the CMIP6 models projected 15–65% increases of LAI by 2100 than present day under the SSP370 scenario (not shown). As a result, inclusion CO_2 effects or not is the largest source of uncertainties for the future projection of isoprene emissions.

There are some limitations in this study. First, we used literature-based observations to validate CMIP6 models but found low

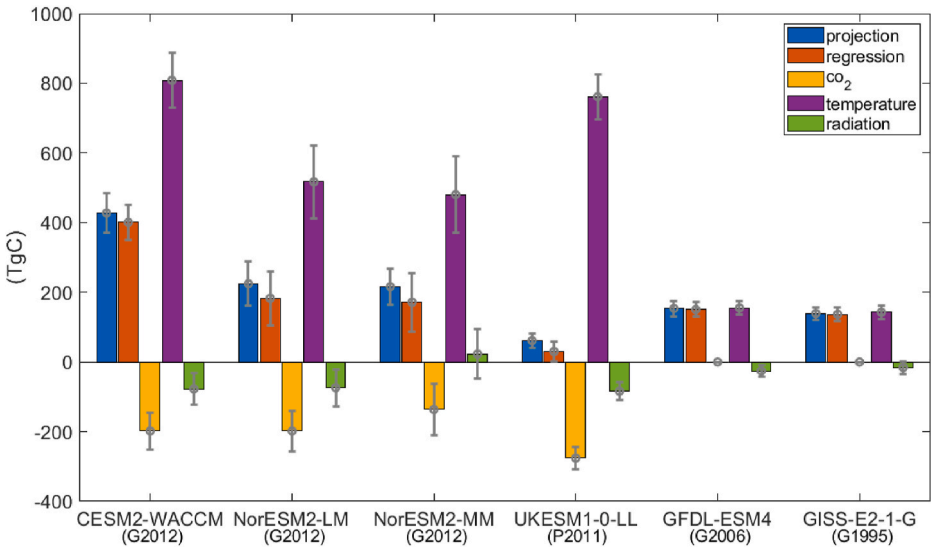

Fig. 5. Changes and attribution of global isoprene emissions at 2080–2100 under SSP370 scenario relative to present day (1990–2010) for six CMIP6 models. The emission changes from CMIP6 model projection (blue), linear regressions (red), and contributions by individual factors including CO_2 (yellow), temperature (purple), and radiation (green) are compared for each model. The errorbar indicates one standard deviation of year-to-year variations. (For interpretation of the references to colour in this figure legend, the reader is referred to the Web version of this article.)

correlations for all models. Such poor performance is partly attributed to the limited observational samples available for model evaluations. More observations are required for better understanding of the spatiotemporal representativeness of isoprene schemes. Second, the regression method considers linear relationships between isoprene emissions and environmental factors, while in reality such relationships are usually nonlinear. In a sensitivity test, we included the interactive term between temperature and radiation into the regression equations (2) and (3) but found limited changes in the driver attributions (Fig. S5). Third, we ignored the influences of LCC in the regression as it remains unclear whether climate models consider LCC and how it is implemented. Finally, the number of available models is still small, which may introduce large uncertainties to the ensemble projections. More models with isoprene emissions are expected for the future projections.

Despite these limitations, our ensemble projection shows 21–57% increases of isoprene emissions by the end of 21st century relative to present day. The enhancement is larger under the warmer scenarios. Since isoprene is an important precursor for surface ozone, which is also sensitive to the changes of temperature, the future threat of ozone pollution likely increases if the anthropogenic emissions are not regulated. Furthermore, isoprene also contributes to the formation of secondary organic aerosol, which is an important component of surface particulate matters. Our projections suggest that more stringent controls of anthropogenic emissions are required to offset the possible increases of surface ozone and particulate matters due to enhanced isoprene emissions in a warmer climate.

CRediT authorship contribution statement

Yang Cao: Data curation, Formal analysis, Writing – original draft. **Xu Yue:** Conceptualization, Supervision, Writing – review & editing. **Hong Liao:** Writing – review & editing, Methodology. **Yang Yang:** Validation. **Jia Zhu:** Data curation. **Lei Chen:** Data curation. **Chenguang Tian:** Data curation. **Yadong Lei:** Data curation. **Hao Zhou:** Data curation. **Yimian Ma:** Data curation.

Declaration of competing interest

The authors declare that they have no known competing financial interests or personal relationships that could have appeared to influence the work reported in this paper.

Acknowledgments

This work was jointly supported by the National Natural Science Foundation of China (Grant No. 41975155), the National Key Research and Development Program of China (Grant No. 2019YFA0606802), and the Startup Foundation for Introducing Talent of NUIST.

Appendix A. Descriptions of parameters used in isoprene algorithms

Name	Description
T_l	leaf temperature (K)
c_{T1}	empirical coefficient (95000 J mol^{-1})
c_{T2}	empirical coefficient (230000 J mol^{-1})
T_S	leaf temperature at a standard condition (e.g., 303 K)
T_M	empirical coefficient (314 K)
R	Constant (8.314 J K^{-1} mol^{-1})
LAI	leaf area index
E_{opt}	empirical coefficients associated with past temperature calculated by Guenther et al. (2006)
C_{T1}	empirical coefficient (95)
C_{T2}	empirical coefficient (230)
x	Function of leaf temperature
a_T	empirical factor (0.1K)
T_a	air temperature
LDF	a light dependent fraction
γ_{T_LDF}	The light-dependent fraction response is calculated following the isoprene-response described by Guenther et al. (2006)

(*continued on next page*)

(*continued*)

Name	Description
γ_{P_LDF}	The light-dependent activity factor described for isoprene by Guenther et al. (2006)
γ_{T_LIF}	The response of the light-independent fraction follows the monoterpene exponential temperature response function of Guenther et al. (2006)
α_1	empirical coefficient (0.0027)
c_{L1}	empirical coefficient (1.066)
Q	flux of PAR ($\mu mol\, m^{-2}s^{-1}$)
C_p	empirical coefficients associated with past PPFD
α	empirical coefficients associated with past PPFD
	leaf level photosynthetic photon flux density ($\mu mol\, m^{-2}s^{-1}$)
A_J	leaf level net photosynthesis when RuBP is limiting
R_D	Leaf level dark respiration
C_i	Leaf internal CO_2 concentration, which is estimated as 70% of the ambient CO_2 concentration
I_{Smax}	empirically coefficient (1.344)
C^*	empirically coefficient (585)
h	empirically coefficient (1.4614)
f_A	The leaf age emission activity factor
f_{SM}	The soil moisture emission activity factor
"*st*" subscript	Variables measured under standard conditions (i.e temperature of 30°C, photosynthetically active radiation of 1000 $\mu mol\, m^{-2}s^{-1}$ and atmospheric CO_2 concentration of 370 ppm)

Appendix B. Supplementary data

Supplementary data to this article can be found online at https://doi.org/10.1016/j.atmosenv.2021.118766.

References

Arneth, A., Miller, P.A., Scholze, M., Hickler, T., Schurgers, G., Smith, B., Prentice, I.C., 2007a. CO2 inhibition of global terrestrial isoprene emissions: potential implications for atmospheric chemistry. Geophys. Res. Lett. 34, 10713–10725. https://doi.org/10.1029/2007gl030615.

Arneth, A., Monson, R.K., Schurgers, G., Niinemets, U., Palmer, P.I., 2008. Why are estimates of global terrestrial isoprene emissions so similar (and why is this not so for monoterpenes)? Atmos. Chem. Phys. 8, 4605–4620. https://doi.org/10.5194/acp-8-4605-2008.

Arneth, A., Niinemets, U., Pressley, S., Back, J., Hari, P., Karl, T., Noe, S., Prentice, I.C., Serca, D., Hickler, T., Wolf, A., Smith, B., 2007b. Process-based estimates of terrestrial ecosystem isoprene emissions: incorporating the effects of a direct CO2-isoprene interaction. Atmos. Chem. Phys. 7, 31–53. https://doi.org/10.5194/acp-7-31-2007.

Atkinson, R., Arey, J., 1998. Atmospheric chemistry of biogenic organic compounds. Acc. Chem. Res. 31, 574–583. https://doi.org/10.1021/ar970143z.

Cheng, S.J., Bohrer, G., Steiner, A.L., Hollinger, D.Y., Suyker, A., Phillips, R.P., Nadelhoffer, K.J., 2015. Variations in the influence of diffuse light on gross primary productivity in temperate ecosystems. Agric. For. Meteorol. 201, 98–110. https://doi.org/10.1016/j.agrformet.2014.11.002.

Claeys, M., Graham, B., Vas, G., Wang, W., Vermeylen, R., Pashynska, V., Cafmeyer, J., Guyon, P., Andreae, M.O., Artaxo, P., Maenhaut, W., 2004. Formation of secondary organic aerosols through photooxidation of isoprene. Science 303, 1173–1176. https://doi.org/10.1126/science.1092805.

Dunne, J.P., Horowitz, L.W., Adcroft, A.J., Ginoux, P., Held, I.M., John, J.G., Krasting, J. P., Malyshev, S., Naik, V., Paulot, F., Shevliakova, E., Stock, C.A., Zadeh, N., Balaji, V., Blanton, C., Dunne, K.A., Dupuis, C., Durachta, J., Dussin, R., Gauthier, P. P.G., Griffies, S.M., Guo, H., Hallberg, R.W., Harrison, M., He, J., Hurlin, W., McHugh, C., Menzel, R., Milly, P.C.D., Nikonov, S., Paynter, D.J., Ploshay, J., Radhakrishnan, A., Rand, K., Reichl, B.G., Robinson, T., Schwarzkopf, D.M., Sentman, L.T., Underwood, S., Vahlenkamp, H., Winton, M., Wittenberg, A.T., Wyman, B., Zeng, Y., Zhao, M., 2020. The GFDL Earth system model version 4.1 (GFDL-ESM 4.1). In: Overall Coupled Model Description and Simulation Characteristics, vol. 12, e2019MS002015. https://doi.org/10.1029/2019MS002015.

Emmons, L., Schwantes, R., Orlando, J., Tyndall, G., Kinnison, D., Lamarque, J.-F., Marsh, D., Mills, M., Tilmes, S., Bardeen, C., Buchholz, R., Conley, A., Gettelman, A., Garcia, R., Simpson, I., Blake, D., Meinardi, S., Pétron, G., 2020. The chemistry mechanism in the community Earth system model version 2 (CESM2). J. Adv. Model. Earth Syst. 12, e2019MS001882 https://doi.org/10.1029/2019MS001882.

Fehsenfeld, F., Calvert, J., Fall, R., Goldan, P., Guenther, A., Hewitt, C., Lamb, B., Liu, S., Trainer, M., Westberg, H., Zimmerman, P., 1992. Emissions of volatile organic compounds from vegetation and the implications for atmospheric chemistry. Global Biogeochem. Cycles 6, 389–430. https://doi.org/10.1029/91gb02965.

Fu, Y., Liao, H., 2012. Simulation of the interannual variations of biogenic emissions of volatile organic compounds in China: impacts on tropospheric ozone and secondary organic aerosol. Atmos. Environ. 59, 170–185. https://doi.org/10.1016/j.atmosenv.2012.05.053.

Ganzeveld, L., Bouwman, L., Stehfest, E., van Vuuren, D.P., Eickhout, B., Lelieveld, J., 2010. Impact of Future Land Use and Land Cover Changes on Atmospheric Chemistry-Climate Interactions, vol. 115. https://doi.org/10.1029/2010JD014041.

Goldstein, A.H., McKay, M., Kurpius, M.R., Schade, G.W., Lee, A., Holzinger, R., Rasmussen, R.A., 2004. Forest thinning experiment confirms ozone deposition to forest canopy is dominated by reaction with biogenic VOCs. Geophys. Res. Lett. 31, L22106. https://doi.org/10.1029/2004gl021259.

Grell, G.A., Peckham, S.E., Schmitz, R., McKeen, S.A., Frost, G., Skamarock, W.C., Eder, B., 2005. Fully coupled "online" chemistry within the WRF model. Atmos. Environ. 39, 6957–6975. https://doi.org/10.1016/j.atmosenv.2005.04.027.

Grote, R., Morfopoulos, C., Niinemets, U., Sun, Z., Keenan, T., Pacifico, F., Butler, T., 2014. A fully integrated isoprenoid emissions model coupling emissions to photosynthetic characteristics. Plant Cell Environ. 37, 1965–1980. https://doi.org/10.1111/pce.12326.

Grote, R., Niinemets, U., 2008. Modeling volatile isoprenoid emissions - a story with split ends. Plant Biol. 10, 8–28. https://doi.org/10.1055/s-2007-964975.

Guenther, A., Gu, D., Yu, H.F., Shilling, J., Shrivastava, M., Karl, T., Artaxo, P., Kaser, L., Santos, F., Longo, K., Martin, S., Yuan, B., Kim, S., Seco, R., 2015. Quantifying regional OH concentrations using airborne measurements of isoprene and its oxidation products. Abstr. Pap. Am. Chem. Soc. 250.

Guenther, A., Hewitt, C.N., Erickson, D., Fall, R., Geron, C., Graedel, T., Harley, P., Klinger, L., Lerdau, M., McKay, W.A., Pierce, T., Scholes, B., Steinbrecher, R., Tallamraju, R., Taylor, J., Zimmerman, P., 1995. A global model of natural volatile organic compound emissions. J. Geophys. Res. Atmos. 100, 8873–8892. https://doi.org/10.1029/94jd02950.

Guenther, A., Jiang, X.Y., Heald, C.L., Sakulyanontvittaya, T., Duhl, T., Emmons, L.K., Wang, X., 2012. The Model of Emissions of Gases and Aerosols from Nature version 2.1 (MEGAN2.1): an extended and updated framework for modeling biogenic emissions. Geosci. Model Dev. (GMD) 5, 1471–1492. https://doi.org/10.5194/gmd-5-1471-2012.

Guenther, A., Karl, T., Harley, P., Wiedinmyer, C., Palmer, P.I., Geron, C., 2006. Estimates of global terrestrial isoprene emissions using MEGAN (model of emissions of gases and aerosols from nature). Atmos. Chem. Phys. 6, 3181–3210. https://doi.org/10.5194/acp-6-3181-2006.

Hantson, S., Knorr, W., Schurgers, G., Pugh, T.A.M., Arneth, A., 2017. Global isoprene and monoterpene emissions under changing climate, vegetation, CO2 and land use. Atmos. Environ. 155, 35–45. https://doi.org/10.1016/j.atmosenv.2017.02.010.

Heald, C.L., Henze, D.K., Horowitz, L.W., Feddema, J., Lamarque, J.F., Guenther, A., Hess, P.G., Vitt, F., Seinfeld, J.H., Goldstein, A.H., Fung, I., 2008. Predicted change in global secondary organic aerosol concentrations in response to future climate, emissions, and land use change. J. Geophys. Res. Atmos. 113 https://doi.org/10.1029/2007jd009092.

Heald, C.L., Wilkinson, M.J., Monson, R.K., Alo, C.A., Wang, G.L., Guenther, A.B., 2009. Response of isoprene emission to ambient CO2 changes and implications for global budgets. Global Change Biol. 15, 1127–1140. https://doi.org/10.1111/j.1365-2486.2008.01802.x.

Hemes, K.S., Verfaillie, J., Baldocchi, D.D., 2020. Wildfire-smoke aerosols lead to increased light use efficiency among agricultural and restored wetland land uses in California's central valley. J. Geophys. Res. Biogeosci. 125 https://doi.org/10.1029/2019JG005380 e2019JG005380.

Henrot, A.J., Stanelle, T., Schroder, S., Siegenthaler, C., Taraborrelli, D., Schultz, M.G., 2017. Implementation of the MEGAN (v2.1) biogenic emission model in the ECHAM6-HAMMOZ chemistry climate model. Geosci. Model Dev. (GMD) 10, 903–926. https://doi.org/10.5194/gmd-10-903-2017.

Horowitz, L.W., Walters, S., Mauzerall, D.L., Emmons, L.K., Rasch, P.J., Granier, C., Tie, X.X., Lamarque, J.F., Schultz, M.G., Tyndall, G.S., Orlando, J.J., Brasseur, G.P., 2003. A global simulation of tropospheric ozone and related tracers: description and evaluation of MOZART, version 2. J. Geophys. Res. Atmos. 108, 29. https://doi.org/10.1029/2002jd002853.

IPCC, 2007. In: Pachauri, R.K., Reisinger, A. (Eds.), Climate Change 2007: Synthesis Report. Contribution of Working Groups I, II and III to the Fourth Assessment Report of the Intergovernmental Panel on Climate Change [Core Writing Team. IPCC, Geneva, Switzerland, p. 104.

IPCC, 2014. In: Pachauri, R.K., Meyer, L.A. (Eds.), Climate Change 2014: Synthesis Report. Contribution of Working Groups I, II and III to the Fifth Assessment Report of the Intergovernmental Panel on Climate Change [Core Writing Team. IPCC, Geneva, Switzerland, p. 151.

Jiang, X.Y., Guenther, A.B., Potosnak, M., Geron, C., Seco, R., Karl, T., Kim, S., Gu, L.H., Pallardy, S., 2018. Isoprene emission response to drought and the impact on global atmospheric chemistry. Atmos. Environ. 183, 69–83. https://doi.org/10.1016/j.atmosenv.2018.01.026.

Kambezidis, H.D., Kaskaoutis, D.G., Kharol, S.K., Moorthy, K.K., Satheesh, S.K., Kalapureddy, M.C.R., Badarinath, K.V.S., Sharma, A.R., Wild, M., 2012. Multi-decadal variation of the net downward shortwave radiation over south Asia: the solar dimming effect. Atmos. Environ. 50, 360–372. https://doi.org/10.1016/j.atmosenv.2011.11.008.

Lamb, B., Pierce, T., Baldocchi, D., Allwine, E., Dilts, S., Westberg, H., Geron, C., Guenther, A., Klinger, L., Harley, P., Zimmerman, P., 1996. Evaluation of forest canopy models for estimating isoprene emissions. J. Geophys. Res. Atmos. 101, 22787–22797. https://doi.org/10.1029/96jd00056.

Lathiere, J., Hauglustaine, D.A., De Noblet-Ducoudre, N., Krinner, G., Folberth, G.A., 2005. Past and future changes in biogenic volatile organic compound emissions simulated with a global dynamic vegetation model. Geophys. Res. Lett. 32 https://doi.org/10.1029/2005gl024164.

Lathiere, J., Hewitt, C.N., Beerling, D.J., 2010. Sensitivity of isoprene emissions from the terrestrial biosphere to 20th century changes in atmospheric CO2 concentration, climate, and land use. Global Biogeochem. Cycles 24, GB1004. https://doi.org/10.1029/2009gb003548.

Levis, S., Wiedinmyer, C., Bonan, G.B., Guenther, A., 2003. Simulating biogenic volatile organic compound emissions in the Community Climate System Model. J. Geophys. Res. Atmos. 108, 4659. https://doi.org/10.1029/2002jd003203.

Li, K., Jacob, D.J., Shen, L., Lu, X., De Smedt, I., Liao, H., 2020. Increases in surface ozone pollution in China from 2013 to 2019: anthropogenic and meteorological influences. Atmos. Chem. Phys. 20, 11423–11433. https://doi.org/10.5194/acp-20-11423-2020.

Liao, H., Chen, W.T., Seinfeld, J.H., 2006. Role of climate change in global predictions of future tropospheric ozone and aerosols. J. Geophys. Res. Biogeosci. 111 https://doi.org/10.1029/2005JD006852. D12304.

Lim, H.J., Carlton, A.G., Turpin, B.J., 2005. Isoprene forms secondary organic aerosol through cloud processing: model simulations. Environ. Sci. Technol. 39, 4441–4446. https://doi.org/10.1021/es048039h.

Lin, G.X., Penner, J.E., Zhou, C., 2016. How will SOA change in the future? Geophys. Res. Lett. 43, 1718–1726. https://doi.org/10.1002/2015gl067137.

Llusia, J., Penuelas, J., Gimeno, B.S., 2002. Seasonal and species-specific response of VOC emissions by Mediterranean woody plant to elevated ozone concentrations. Atmos. Environ. 36, 3931–3938. https://doi.org/10.1016/s1352-2310(02)00321-7.

Muller, J.F., Stavrakou, T., Wallens, S., De Smedt, I., Van Roozendael, M., Potosnak, M.J., Rinne, J., Munger, B., Goldstein, A., Guenther, A.B., 2008. Global isoprene emissions estimated using MEGAN, ECMWF analyses and a detailed canopy environment model. Atmos. Chem. Phys. 8, 1329–1341. https://doi.org/10.5194/acp-8-1329-2008.

Niinemets, U., Tenhunen, J.D., Harley, P.C., Steinbrecher, R., 1999. A model of isoprene emission based on energetic requirements for isoprene synthesis and leaf photosynthetic properties for Liquidambar and Quercus. Plant Cell Environ. 22, 1319–1335. https://doi.org/10.1046/j.1365-3040.1999.00505.x.

Ortega, J., Helmig, D., Guenther, A., Harley, P., Pressley, S., Vogel, C., 2007. Flux estimates and OH reaction potential of reactive biogenic volatile organic compounds (BVOCs) from a mixed northern hardwood forest. Atmos. Environ. 41, 5479–5495. https://doi.org/10.1016/j.atmosenv.2006.12.033.

Pacifico, F., Folberth, G.A., Jones, C.D., Harrison, S.P., Collins, W.J., 2012. Sensitivity of biogenic isoprene emissions to past, present, and future environmental conditions and implications for atmospheric chemistry. J. Geophys. Res. Atmos. 117, D22302. https://doi.org/10.1029/2012jd018276.

Pacifico, F., Harrison, S.P., Jones, C.D., Arneth, A., Sitch, S., Weedon, G.P., Barkley, M.P., Palmer, P.I., Serca, D., Potosnak, M., Fu, T.M., Goldstein, A., Bai, J.H., Schurgers, G., 2011. Evaluation of a photosynthesis-based biogenic isoprene emission scheme in JULES and simulation of isoprene emissions under present-day climate conditions. Atmos. Chem. Phys. 11, 4371–4389. https://doi.org/10.5194/acp-11-4371-2011.

Pacifico, F., Harrison, S.P., Jones, C.D., Sitch, S., 2009. Isoprene emissions and climate. Atmos. Environ. 43, 6121–6135. https://doi.org/10.1016/j.atmosenv.2009.09.002.

Penuelas, J., Staudt, M., 2010. BVOCs and global change. Trends Plant Sci. 15, 133–144. https://doi.org/10.1016/j.tplants.2009.12.005.

Piao, S.L., Sitch, S., Ciais, P., Friedlingstein, P., Peylin, P., Wang, X.H., Ahlstrom, A., Anav, A., Canadell, J.G., Cong, N., Huntingford, C., Jung, M., Levis, S., Levy, P.E., Li, J.S., Lin, X., Lomas, M.R., Lu, M., Luo, Y.Q., Ma, Y.C., Myneni, R.B., Poulter, B., Sun, Z.Z., Wang, T., Viovy, N., Zaehle, S., Zeng, N., 2013. Evaluation of terrestrial carbon cycle models for their response to climate variability and to CO2 trends. Global Change Biol. 19, 2117–2132. https://doi.org/10.1111/gcb.12187.

Possell, M., Hewitt, C.N., 2011. Isoprene emissions from plants are mediated by atmospheric CO2 concentrations. Global Change Biol. 17, 1595–1610. https://doi.org/10.1111/j.1365-2486.2010.02306.x.

Possell, M., Hewitt, C.N., Beerling, D.J., 2005. The effects of glacial atmospheric CO2 concentrations and climate on isoprene emissions by vascular plants. Global Change Biol. 11, 60–69. https://doi.org/10.1111/j.1365-2486.2004.00889.x.

Rabin, S.S., Alexander, P., Henry, R., Anthoni, P., Pugh, T.A.M., Rounseyell, M., Arneth, A., 2020. Impacts of future agricultural change on ecosystem service indicators. Earth Syst. Dynam. 11, 357–376. https://doi.org/10.5194/esd-11-357-2020.

Rinne, J., Guenther, A., Greenberg, J., Harley, P., 2002. Isoprene and monoterpene fluxes measured above Amazonian rainforest and their dependence on light and temperature. Atmos. Environ. 36, 2421–2426. https://doi.org/10.1016/s1352-2310(01)00523-4.

Sanderson, M.G., Jones, C.D., Collins, W.J., Johnson, C.E., Derwent, R.G., 2003. Effect of climate change on isoprene emissions and surface ozone levels. Geophys. Res. Lett. 30, 1936. https://doi.org/10.1029/2003GL017642.

Sellar, A.A., Jones, C.G., Mulcahy, J.P., Tang, Y.M., Yool, A., Wiltshire, A.J., O'Connor, F. M., Stringer, M., Hill, R., Palmieri, J., Woodward, S., de Mora, L., Kuhlbrodt, T., Rumbold, S.T., Kelley, D.I., Ellis, R., Johnson, C.E., Walton, J., Abraham, N.L., Andrews, M.B., Andrews, T., Archibald, A.T., Berthou, S., Burke, E., Blockley, E., Carslaw, K., Dalvi, M., Edwards, J., Folberth, G.A., Gedney, N., Griffiths, P.T., Harper, A.B., Hendry, M.A., Hewitt, A.J., Johnson, B., Jones, A., Jones, C.D., Keeble, J., Liddicoat, S., Morgenstern, O., Parker, R.J., Predoi, V., Robertson, E., Siahaan, A., Smith, R.S., Swaminathan, R., Woodhouse, M.T., Zeng, G., Zerroukat, M., 2019. UKESM1: description and evaluation of the U.K. Earth system model. J. Adv. Model. Earth Syst. 11, 4513–4558. https://doi.org/10.1029/2019MS001739.

Sharkey, T.D., Loreto, F., 1993. Water-stress, temperature, and light effects on the capacity for isoprene emission and photosynthesis of kudzu leaves. Oecologia 95, 328–333. https://doi.org/10.1007/bf00320984.

Sharkey, T.D., Singsaas, E.L., Vanderveer, P.J., Geron, C., 1996. Field measurements of isoprene emission from trees in response to temperature and light. Tree Physiol. 16, 649–654. https://doi.org/10.1093/treephys/16.7.649.

Shindell, D.T., Faluvegi, G., Unger, N., Aguilar, E., Schmidt, G.A., Koch, D.M., Bauer, S. E., Miller, R.L., 2006. Simulations of preindustrial, present-day, and 2100 conditions in the NASA GISS composition and climate model G-PUCCINI. Atmos. Chem. Phys. 6, 4427–4459. https://doi.org/10.5194/acp-6-4427-2006.

Situ, S., Guenther, A., Wang, X., Jiang, X., Turnipseed, A., Wu, Z., Bai, J., Wang, X., 2013. Impacts of seasonal and regional variability in biogenic VOC emissions on surface ozone in the Pearl River delta region, China. Atmos. Chem. Phys. 13, 11803–11817. https://doi.org/10.5194/acp-13-11803-2013.

Squire, O.J., Archibald, A.T., Abraham, N.L., Beerling, D.J., Hewitt, C.N., Lathiere, J., Pike, R.C., Telford, P.J., Pyle, J.A., 2014. Influence of future climate and cropland expansion on isoprene emissions and tropospheric ozone. Atmos. Chem. Phys. 14, 1011–1024. https://doi.org/10.5194/acp-14-1011-2014.

Stavrakou, T., Muller, J.F., Bauwens, M., De Smedt, I., Van Roozendael, M., Guenther, A., Wild, M., Xia, X., 2014. Isoprene emissions over Asia 1979-2012: impact of climate and land-use changes. Atmos. Chem. Phys. 14, 4587–4605. https://doi.org/10.5194/acp-14-4587-2014.

Szogs, S., Arneth, A., Anthoni, P., Doelman, J.C., Humpenoeder, F., Popp, A., Pugh, T.A. M., Stehfest, E., 2017. Impact of LULCC on the emission of SVOCs during the 21st century. Atmos. Environ. 165, 73–87. https://doi.org/10.1016/j.atmosenv.2017.06.025.

Tai, A.P.K., Mickley, L.J., Heald, C.L., Wu, S.L., 2013. Effect of CO2 inhibition on biogenic isoprene emission: implications for air quality under 2000 to 2050 changes in climate, vegetation, and land use. Geophys. Res. Lett. 40, 3479–3483. https://doi.org/10.1002/grl.50650.

Tai, A.P.K., Mickley, L.J., Jacob, D.J., Leibensperger, E.M., Zhang, L., Fisher, J.A., Pye, H. O.T., 2012. Meteorological modes of variability for fine particulate matter (PM2.5) air quality in the United States: implications for PM2.5 sensitivity to climate change. Atmos. Chem. Phys. 12, 3131–3145. https://doi.org/10.5194/acp-12-3131-2012.

Tingey, D.T., Manning, M., Grothaus, L.C., Burns, W.F., 1979. Influence of light and temperature on isoprene emission rates from live oak. Physiol. Plantarum 47, 112–118. https://doi.org/10.1111/j.1399-3054.1979.tb03200.x.

Unger, N., Harper, K., Zheng, Y., Kiang, N.Y., Aleinov, I., Arneth, A., Schurgers, G., Amelynck, C., Goldstein, A., Guenther, A.B., Heinesch, B., Hewitt, C.N., Karl, T., Laffineur, Q., Langford, B., McKinney, K.A., Misztal, P., Potosnak, M., Rinne, J., Pressley, S., Schoon, N., Seraca, D., 2013. Photosynthesis-dependent isoprene emission from leaf to planet in a global carbon-chemistry-climate model. Atmos. Chem. Phys. 13, 10243–10269. https://doi.org/10.5194/acp-13-10243-2013.

Velikova, V., Pinelli, P., Pasqualini, S., Reale, L., Ferranti, F., Loreto, F., 2005. Isoprene decreases the concentration of nitric oxide in leaves exposed to elevated ozone. New Phytol. 166, 419–426. https://doi.org/10.1111/j.1469-8137.2005.01409.x.

Wang, L., Tai, A.P.K., Tam, C.Y., Sadiq, M., Wang, P., Cheung, K.K.W., 2020. Impacts of future land use and land cover change on mid-21st-century surface ozone air quality: distinguishing between the biogeophysical and biogeochemical effects. Atmos. Chem. Phys. 20, 11349–11369. https://doi.org/10.5194/acp-20-11349-2020.

Wang, Y.H., Jacob, D.J., Logan, J.A., 1998. Global simulation of tropospheric O3-NO x -hydrocarbon chemistry: 1. Model formulation. Journal of Geophysical Research Atmospheres 103, 10713–10725. https://doi.org/10.1029/98JD00158.

Wiedinmyer, C., Tie, X., Guenther, A., Neilson, R., Granier, C., 2006. Future changes in biogenic isoprene emissions: how might they affect regional and global atmospheric chemistry? Earth Interact. 10 https://doi.org/10.1175/ei174.1.

Wild, M., 2009. Global dimming and brightening: a review. J. Geophys. Res. Atmos. 114, 31. https://doi.org/10.1029/2008jd011470.

Wilkinson, M.J., Monson, R.K., Trahan, N., Lee, S., Brown, E., Jackson, R.B., Polley, H. W., Fay, P.A., Fall, R., 2009. Leaf isoprene emission rate as a function of atmospheric CO2 concentration. Global Change Biol. 15, 1189–1200. https://doi.org/10.1111/j.1365-2486.2008.01803.x.

Wu, S., Mickley, L.J., Kaplan, J.O., Jacob, D.J., 2012. Impacts of changes in land use and land cover on atmospheric chemistry and air quality over the 21st century. Atmos. Chem. Phys. 12, 1597–1609. https://doi.org/10.5194/acp-12-1597-2012.

Young, P.J., Arneth, A., Schurgers, G., Zeng, G., Pyle, J.A., 2009. The CO2 inhibition of terrestrial isoprene emission significantly affects future ozone projections. Atmos. Chem. Phys. 9, 2793–2803. https://doi.org/10.5194/acp-9-2793-2009.

Yue, X., Unger, N., Zheng, Y., 2015. Distinguishing the drivers of trends in land carbon fluxes and plant volatile emissions over the past 3 decades. Atmos. Chem. Phys. 15, 11931–11948. https://doi.org/10.5194/acp-15-11931-2015.

Yukimoto, S., Kawai, H., Koshiro, T., Oshima, N., Yoshida, K., Urakawa, S., Tsujino, H., Deushi, M., Tanaka, T., Hosaka, M., Yabu, S., Yoshimura, H., Shindo, E., Mizuta, R., Obata, A., Adachi, Y., Ishii, M., 2019. The meteorological Research Institute Earth system model version 2.0, MRI-ESM2.0: description and basic evaluation of the physical component. Journal of the Meteorological Society of Japan. Ser. II 97, 931–965. https://doi.org/10.2151/jmsj.2019-051.